J|A|C|S
ARTICLES
Published on Web 08/02/2002

# Density Functional Study of the Mechanism of a Tyrosine Phosphatase: I. Intermediate Formation

Dilipkumar Asthagiri,[†,§] Valerie Dillet,[†] Tiqing Liu,[†] Louis Noodleman,[†] Robert L. Van Etten,[‡] and Donald Bashford*[,†]

*Contribution from the Department of Molecular Biology, TPC-15, The Scripps Research Institute, 10550 North Torrey Pines Road, La Jolla, California 92037, and Department of Chemistry, Purdue University, West Lafayette, Indiana 47907-1393*

Received January 9, 2002. Revised Manuscript Received May 23, 2002

***Abstract:*** The first step in the catalytic mechanism of a protein tyrosine phosphatase, the transfer of a phosphate group from the phosphotyrosine substrate to a cysteine side chain of the protein to form a phosphoenzyme intermediate, has been studied by combining density functional calculations of an active-site cluster with continuum electrostatic descriptions of the solvent and the remainder of the protein. This approach provides the high level of quantum chemical methodology needed to adequately model phosphotransfer reactions with a reasonable description of the environment around the active site. Energy barriers and geometries along a reaction pathway are calculated. In the literature, mechanisms assuming both a monoanionic and a dianionic substrate have been proposed; this disagreement is addressed by performing calculations for both possibilities. For the dianionic substrate, a dissociative reaction pathway with early proton transfer to the leaving group and a 9 kcal/mol energy barrier is predicted (the experimental estimate is ca. 14 kcal/mol), while for the monoanionic substrate, an associative pathway with late proton transfer and a 22 kcal/mol energy barrier is predicted. These results, together with a review of experimental evidence, support the dianionic-substrate/dissociative-pathway alternative. The relationship between a dianionic or monoanionic substrate and a dissociative or associative pathway, respectively, can be understood in terms of classical organic chemical reaction pathways.

## 1. Introduction

The protein tyrosine phosphatases (PTPases), which complement the kinases in their physiological action,[1] are characterized by a vast structural diversity, but all of them share a conserved active site structure comprising the (H/V)C(X)$_5$R(S/T) residues, termed the phosphate binding loop or the P-loop.[2] The strict conservation of the active site suggests that the chemical steps in catalysis are the same for all members of the PTPase family. The phosphoryl transfer occurs in two steps (see ref 2 and references therein). In the first step, the catalytic cysteine residue of the P-loop abstracts the phosphoryl group forming a phosphoenzyme intermediate, while a conserved aspartic acid side chain from outside the P-loop donates a proton to the oxygen of the leaving tyrosyl group. In the subsequent step, this phosphoenzyme intermediate is hydrolyzed to release an inorganic phosphate and regenerate the enzyme. In this paper, we present our investigation of the first step of the mechanism. Although there is general agreement regarding the two-step phosphoryl transfer, there is disagreement regarding the exact mechanism. The first proposition (see, for example, ref 2), mechanism A, reads:

$$ES^- + ROPO_3^{2-} \rightleftharpoons [ES{\cdot}PO_3RO]^{3-}$$

$$ECOOH + [ES{\cdot}PO_3RO]^{3-} \rightarrow ECOO^- + ESPO_3^{2-} + ROH$$

Here $[ES{\cdot}PO_3RO]^{3-}$ represents the Michaelis complex. The catalytic cysteine residue in the enzyme (E) exists as a thiolate ($S^-$). The substrate, $ROPO_3^{2-}$, binds to the enzyme in the dianionic form. The nucleophilic attack is thought to displace the phenoxide anion, which is protonated by the conserved general acid, ECOOH, to be released as phenol.

An alternative,[3−5] mechanism B, argues against the −3 charge in the Michaelis complex and instead proposes that the substrate binds to the enzyme in the monoanionic form. Thus

$$ES^- + ROPO_3H^- \rightleftharpoons [ES{\cdot}PO_3HRO]^{2-}$$

$$ECOOH + [ES{\cdot}PO_3HRO]^{2-} \rightarrow ECOO^- + ESPO_3H^- + ROH$$

* To whom correspondence should be addressed. E-mail: bashford@scripps.edu. Fax: +1-858-784-8896.
† The Scripps Research Institute.
‡ Purdue University.
§ Present address: Group T-12, MS-B268, Los Alamos National Laboratory, Los Alamos, NM 87544.

(1) Fischer, E. H.; Charbonneau, H.; Tonks, N. K. *Science* **1991**, *253*, 401.
(2) Jackson, M. D.; Denu, J. M. *Chem. Rev.* **2001**, *101*, 2313.
(3) Hansson, T.; Nordlund, P.; Åqvist, J. *J. Mol. Biol.* **1997**, *265*, 118.
(4) Kolmodin, K.; Nordlund, P.; Åqvist, J. *Protein: Struct., Funct., Genet.* **1999**, *36*, 370.
(5) Kolmodin, K.; Åqvist, J. *Int. J. Quantum Chem.* **1999**, *73*, 147.

10.1021/ja020046n CCC: $22.00 

As in mechanism A, the displaced phenoxide anion is protonated by the general acid. A variant of this mechanism,[3−5] mechanism B′, which considers the existence of the cysteine in the thiol form, suggests:

$$ESH + ROPO_3^{2-} \rightarrow ES^- + ROPO_3H^-$$

$$ES^- + ROPO_3H^- \rightleftharpoons [ES{\cdot}PO_3HRO]^{2-}$$

$$ECOOH + [ES{\cdot}PO_3HRO]^{2-} \rightarrow ECOO^- + ESPO_3H^- + ROH$$

Thus, the dianionic substrate, acting as a base, activates the thiol to a thiolate by abstracting the proton. Thereafter, the reaction proceeds according to mechanism B. One of the three nonbridging oxygens of the substrate is thought to abstract the proton. A common feature of mechanisms B and B′ is the net charge of −2 in the Michaelis complex versus −3 for mechanism A.

In a wide variety of phosphatases, the protonation states in mechanism A are widely supported by pH-dependence of $k_{cat}/K_m$[6−9] and by assays that probe the thiolate nature of the cysteine nucleophile.[7,10] Further, that the conserved aspartate is protonated and functions as the general acid has been inferred from experimental pH-dependence data[6−9] and mutations of Asp 129 in the low molecular weight phosphatase,[11] and by theoretical calculations.[12] However, in the case of the low molecular weight bovine PTPase,[13] because of likely enzyme denaturation at low pH, an unambiguous assignment of protonation states was not possible. An important requirement of mechanism A is the existence of the nucleophile in the thiolate form in the free protein and in the Michaelis complex. Theoretical calculations by Dillet et al.[12] explored how the enzyme can achieve this via a unique arrangement of P-loop dipoles and protein secondary structural elements. However, despite these stabilizing interactions, it is unclear how and why nature chooses the dianionic state of the substrate, if in fact it does, to be attacked by a thiolate. After all, nucleophilic attack seemingly would be more facile if the substrate were monoanionic, as in mechanism B or the "activated" stages of B′.

Mechanism B seems intuitively the more reasonable alternative if we posit that nucleophilic attack leads to the displacement and subsequent protonation of the phenolic leaving group. However, this alternative calls into question much of the accepted experimental studies on PTPases. Indeed, the proponents of this scheme[4,5] have questioned the experimental assignment of ionization constants based on pH-dependence of kinetics and also the interpretations based on kinetic isotope effects. Flaws in these criticisms and clarifications of earlier experiments were subsequently presented by Cyzyrca and Hengge.[14] Mechanism B′ is attractive if one posits that (a) the enzyme cannot shift the p$K_a$ of the cysteine thiol so as to make it a thiolate, and (b) the substrate is dianionic as the pH-dependence of enzyme kinetics suggests. Similar proposals involving substrate activation have been made both for solution hydrolysis of phosphate monoesters[15] and for enzymatic hydrolysis of GTP.[16] However, such substrate-activation in phosphoryl transfer reactions has been shown to be highly unlikely purely on the basis of kinetic arguments,[17] and, in phosphatases, kinetic isotope effects do not seem to support them either.[14,18] Thus, we have the following problem: On one hand, nature apparently adopts mechanism A, but nucleophilic attack by a −1 charged thiolate on a −2 charged substrate is troubling if not counterintuitive. On the other, it is unclear why nature does not adopt mechanism B (or B′), if this indeed is the case. This is the principal question addressed in this paper.

The mechanistic studies by Åqvist and co-workers[3−5] using the empirical valence bond approach drew them to conclude that mechanisms B or B′ are energetically most favorable. An AM1/MNDO semiempirical quantum mechanics treatment of the nucleophile, substrate, and general acid in a protein matrix described by molecular mechanics using the PARAM22 force field[19] in CHARMM[20] led Gao and co-workers[21] to conclude in favor of mechanism A. Yet they failed to predict the protonation of the leaving phenoxide group. Czyryca and Hengge[14] using the PM3 semiempirical Hamiltonian and a large (nearly 300 atom) quantum cluster modeled the pathway for mechanism A. Their focus was primarily on the structural evolution. They predict a concerted phosphoryl transfer, the bond-breaking and bond-forming processes occur concurrently, and the transition state is dissociative. Because of the noninclusion of long-range electrostatics and solvation effects, their barrier heights could not be compared with experiments.

In the present approach, we use high-level density functional methods of quantum chemistry to study the mechanisms. We treat a select group of protein atoms as part of the quantum cluster and compute a reaction path. The energetics and electron density distribution are then recalculated self-consistently in the presence of the entire protein and solvent. A high-level quantum chemical approach, which is probably essential for accurate descriptions of phosphate chemistry (see ref 22 and references therein), and allowance for electronic density polarization due to the protein and solvent are distinguishing aspects of this work, and, to the best of our knowledge, is the first such study of a PTPase. We compute the reaction path for both mechanisms A and B and conclude with an analysis of our results from structural, energetic, and organic chemical perspectives.

(6) Zhang, Z. Y.; Malachowski, W. P.; Van Etten, R. L.; Dixon, J. E. *J. Biol. Chem.* **1994**, *269*, 8140.
(7) Denu, J. M.; Zhou, G.; Guo, Y.; Dixon, J. E. *Biochemistry* **1995**, *34*, 3396.
(8) Denu, J. M.; Dixon, J. E. *Proc. Natl. Acad. Sci. U.S.A.* **1995**, *92*, 5910.
(9) Lohse, D. L.; Denu, J. M.; Santoro, N.; Dixon, J. E. *Biochemistry* **1997**, *36*, 4568.
(10) Zhang, Z. Y.; Dixon, J. E. *Biochemistry* **1993**, *32*, 9340.
(11) Zhang, Z.; Harms, E.; Van Etten, R. L. *J. Biol. Chem.* **1994**, *269*, 25947.
(12) Dillet, V.; Van Etten, R. L.; Bashford, D. *J. Phys. Chem. B* **2000**, *104*, 11321.
(13) Evans, B.; Tishmack, P. A.; Pokalsky, C.; Zhang, M.; Van Etten, R. L. *Biochemistry* **1996**, *35*, 13609.
(14) Czyryca, P. G.; Hengge, A. C. *Biochim. Biophys. Acta* **2001**, *1547*, 245.
(15) Florian, J.; Warshel, A. *J. Am. Chem. Soc.* **1997**, *119*, 5473.
(16) Schweins, T.; Langen, R.; Warshel, A. *Nat. Struct. Biol.* **1994**, *1*, 476.
(17) Admiraal, S. J.; Herschlag, D. *J. Am. Chem. Soc.* **2000**, *122*, 2145.
(18) Hengge, A. C. *Acc. Chem. Res.* **2002**, *35*, 105.
(19) MacKerell, A. D., Jr.; Bashford, D.; Bellott, M.; Dunbrack, R. L., Jr.; Evanseck, J. D.; Field, M. J.; Fischer, S.; Gao, J.; Guo, H.; Ha, S.; Joseph-McCarthy, D.; Kuchnir, L.; Kuczera, K.; Lau, F. T. K.; Mattos, C.; Michnick, S.; Ngo, T.; Nguyen, D. T.; Prod'hom, B.; Reiher, W. E., III; Roux, B.; Schlenkrich, M.; Smith, J. C.; Stote, R.; Straub, J.; Watanabe, M.; Wiorkiewicz-Kuczera, J.; Yin, D.; Karplus, M. *J. Phys. Chem. B* **1998**, *102*, 3586.
(20) Brooks, B. R.; Bruccoleri, R. E.; Olafson, B. D.; States, D. J.; Swaminathan, S.; Karplus, M. *J. Comput. Chem.* **1983**, *4*, 187.
(21) Alhambra, C.; Wu, L.; Zhang, Z. Y.; Gao, J. *J. Am. Chem. Soc.* **1998**, *120*, 3858.
(22) Dejaegere, A.; Liang, X.; Karplus, M. *J. Chem. Soc., Faraday Trans.* **1994**, *90*, 1763.

***Table 1.*** Important Geometrical Parameters of the Molecular Mechanics Energy-Minimized Starting Structure[a]

| mechanism | R(P–S) | $R(O_B–H_A)$ | $R(S–H_\gamma)$ | $\angle O_BPS$ |
|---|---|---|---|---|
| A | 3.8 | 2.01 | 2.11 | 176.4 |
| B | 3.8 | 2.00 | 2.15 | 161.1 |

[a] Bond lengths are in Å, and bond angles are in degrees. The atom names are as in Figure 1.

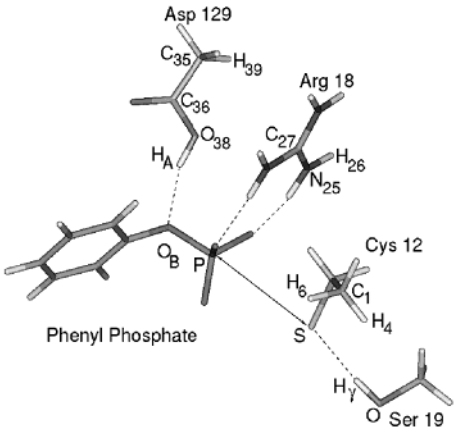


***Figure 1.*** Schematic of the quantum cluster. H-bonding interactions are shown by broken lines. The P−S distance is the reaction coordinate.

## 2. Methods

**Structural Model.** The structure of bovine protein tyrosine phosphatase (BPTP) complexed with a model phenyl phosphate structure was kindly provided by Marie Zhang (Purdue). This structure is similar to 1PNT found in the PDB,[23] but with a phenyl phosphate modeled in place of the HEPES ligand. Hydrogen atom coordinates were generated using HBUILD[24] within the CHARMM (version c26b2) package[20] using the PARAM22[19] force field parameters. All Arg, Lys, and His residues were protonated. This protonation state of the His residues is consistent with direct experimental measurements.[25] Glu and Asp residues, except the general acid Asp 129, were deprotonated, the nucleophilic cysteine was modeled as a thiolate, and the substrate, phenyl phosphate, was modeled in both the deprotonated, dianionic (−2) and the protonated, monoanionic (−1) forms. The parameters for the substrate were as described earlier by Dillet et al.[12]

Structure refinement included an initial 200 steps of steepest-descent energy minimization in the absence of electrostatic interactions. Next the structures were energy-minimized using the conjugate-gradient energy minimizer including electrostatic interactions (13.0 Å cutoff and dielectric constant of 4.0). During minimization, all of the atoms were allowed to move. At convergence, the RMS deviations between the initial and energy-minimized structures were less than 0.75 Å. Table 1 lists pertinent geometric information obtained after energy-minimization.

**Quantum Cluster.** The quantum cluster is excised from the energy-minimized structure (Figure 1). The cysteine residue was modeled as an ethanethiolate by replacing the bonds between $C_\alpha$ and the backbone N and C atoms by $C_\alpha$−H bonds. Ser 19 was modeled as methanol; the bond between $C_\beta$ and $C_\alpha$ was replaced by a $C_\beta$−H bond. Arg 18 was modeled as a guanidinium ion; the bond between $N_\epsilon$ and $C_\delta$ was replaced by a $N_\epsilon$−H bond. Asp 129 was modeled as acetic acid; the bond between $C_\beta$ and $C_\alpha$ was replaced by a $C_\beta$−H bond. These replacements with hydrogen "linking" atoms were performed within the InsightII modeling program, and the heavy-atom link-hydrogen bond length was set at 1 Å. In all, the cluster comprised 48 atoms for mechanism A and 49 atoms for mechanism B.

***Table 2.*** Calculated Heat of Reaction (kcal/mol) Including Thermal Vibrational Terms for the Model Reactions 1 and 2[a]

| | Alhambra et al. | | | this work | | |
|---|---|---|---|---|---|---|
| | expt[b] | AM1/MNDO | MP2[d] | VWN(Stoll) | B3LYP[e] | PW91[f] |
| rxn 1 | 10.5[c] | 17.2 | 16.0 | 16.7 (19.8) | 16.0 (19.1) | 13.8 (16.9) |
| rxn 2 | −1.6 | 5.5 | −2.5 | −2.4 (−2.4) | −2.1 (−2.1) | −3.2 (−3.2) |

[a] Values in parentheses are the purely electronic change in energy. [b] Experimental values reported by Alhambra et al.[21] [c] Estimated by Alhambra et al.[21] using Benson's rules. [d] MP2/6-31+G(d,p). [e] B3LYP/6-311+G(d,p) energy calculations with VWN(Stoll)-optimized geometry. [f] PW91 energy calculations with basis sets and geometries as in the VWN(Stoll) calculations. Vibrational corrections were calculated with the VWN(Stoll) functional.

**DFT Calculations.** The Amsterdam density functional (ADF) program (version 2.3)[26] was used for the reaction path calculations. The density functional that we chose represented a compromise between reliable prediction of heats of reaction for model systems, on one hand, and speed of computing, on the other. Thus, we chose the local density approximation (LDA) for the exchange and correlation functional on the basis of the parametrization of Vosko, Wilk, and Nusair (VWN)[27] and the correlation correction defined by Stoll.[28,29] To test this approach in comparison to functionals including gradient corrections and hybrid density functionals such as B3LYP,[30] which are computationally expensive, we performed calculations on the model reactions used by Alhambra et al.:[21]

$$CH_3OPO_3^{=} + CH_3S^- \rightarrow CH_3O^- + CH_3SPO_3^{=} \qquad \text{rxn 1}$$

$$C_6H_5O^- + CH_3COOH \rightarrow C_6H_5OH + CH_3COO^- \qquad \text{rxn 2}$$

The calculated gas phase heats of reaction at various levels of theory are shown in Table 2. The excellent agreement between calculations using the VWN(Stoll) functional and B3LYP[30] hybrid functional suggests that this functional is adequate for the present study of phosphoryl transfer. The Gaussian 98 programs[31] were used for calculations with B3LYP. The PW91[32] results are also quite similar to those using the VWN(Stoll) and B3LYP functionals. Note that the AM1/MNDO Hamiltonian used by Alhambra et al.[21] predicts that reaction 2 above is endothermic. We correctly predict that the reaction is exothermic, as they find using MP2 level calculations. This inaccuracy likely leads to their inability to predict the proton transfer from Asp 129 to the leaving phenoxide anion.

The basis sets in our calculations were formed from double-ζ Slater-type orbitals (STO) for H, C, N, and O atoms, and triple-ζ STOs for the P and S atoms. A polarization function (single-ζ, 3d) was added

(23) Berman, H. M.; Westbrook, J.; Feng, Z.; Gilliland, G.; Bhat, T. N.; Weissig, H.; Shindyalov, I. N.; Bourne, P. E. *Nucleic Acids Res.* **2000**, *28*, 235.
(24) Brünger, A. T.; Karplus, M. *Proteins: Struct., Funct., Genet.* **1988**, *4*, 148.
(25) Tishmack, P. A.; Bashford, D.; Harms, E.; Van Etten, R. L. *Biochemistry* **1997**, *36*, 11984.
(26) Guerra, C. F.; Snijders, J. G.; te Velde, G.; Baerends, E. J. *Theor. Chem. Acc.* **1998**, *99*, 391.
(27) Vosko, S. H.; Wilk, L.; Nusair, M. *Can. J. Phys.* **1980**, *58*, 1200.
(28) Stoll, H.; Pavlidou, C. M. E.; Preuss, H. *Theor. Chim. Acta* **1978**, *49*, 143.
(29) Stoll, H.; Golka, E.; Preuss, H. *Theor. Chim. Acta* **1980**, *55*, 29.
(30) Becke, A. D. *J. Chem. Phys.* **1993**, *98*, 5648.
(31) Frisch, M. J.; Trucks, G. W.; Schlegel, H. B.; Scuseria, G. E.; Robb, M. A.; Cheeseman, J. R.; Zakrzewski, V. G.; Montgomery, J. A., Jr.; Stratmann, R. E.; Burant, J. C.; Dapprich, S.; Millam, J. M.; Daniels, A. D.; Kudin, K. N.; Strain, M. C.; Farkas, O.; Tomasi, J.; Barone, V.; Cossi, M.; Cammi, R.; Mennucci, B.; Pomelli, C.; Adamo, C.; Clifford, S.; Ochterski, J.; Petersson, G. A.; Ayala, P. Y.; Cui, Q.; Morokuma, K.; Malick, D. K.; Rabuck, A. D.; Raghavachari, K.; Foresman, J. B.; Cioslowski, J.; Ortiz, J. V.; Stefanov, B. B.; Liu, G.; Liashenko, A.; Piskorz, P.; Komaromi, I.; Gomperts, R.; Martin, R. L.; Fox, D. J.; Keith, T.; Al-Laham, M. A.; Peng, C. Y.; Nanayakkara, A.; Gonzalez, C.; Challacombe, M.; Gill, P. M. W.; Johnson, B.; Chen, W.; Wong, M. W.; Andres, J. L.; Gonzalez, C.; Head-Gordon, M.; Replogle, E. S.; Pople, J. A. *Gaussian 98*, revision A.7; Gaussian, Inc.: Pittsburgh, PA, 1998.
(32) Perdew, J. P.; Chevary, J. A.; Vosko, S. H.; Jackson, K. A.; Pederson, M. R.; Singh, D. J.; Fiolhais, C. *Phys. Rev. B* **1992**, *46*, 6671.

for the sulfur, the phosphorus, and the four substrate oxygen atoms. The inner core electrons (1s for atoms C, N, O and 1s, 2s, 2p for atoms S, P) were described by the frozen core approximation.

**Reaction Path Calculations.** The geometry optimizations used a quasi-Newton approach with the Broyden−Fletcher−Goldfarb−Shanno[33] scheme for Hessian updating. Convergence tolerance required that the change in energy (in hartrees), gradients, bond lengths (in Å), and angles (in degrees) be simultaneously less than $10^{-3}$ H, $5 \times 10^{-3}$ H/Å, 0.01 Å, and 0.5°, respectively. The SCF convergence was specified such that convergence was considered reached when the maximum element of the commutator of the Fock matrix and the density matrix fell below $10^{-4}$.

During geometry optimization, some degrees of freedom were constrained to (a) maintain a reasonable approximation to the active site geometry and (b) to reduce computational cost. Atoms of the ethanethiolate group were not allowed to move. The methyl group in methanol was fixed, but the hydroxyl O and H atoms were free. The positions of the phosphorus atom, the equatorial oxygen atoms, and the $O_B$ atom were fully unconstrained. Thus, the bond that is broken during the first step of the catalytic process ($P-O_B$) (Figure 1) was free to change. The phenyl ring was internally constrained, although it could move relative to the P atom, and the angle formed by $O_B-P-S$ was constrained to the initial value (Table 1) to represent the restrictions on the substrate orientation imposed by the active-site pocket. The internal degrees of freedom of the guanidinium ion were frozen, but rotation about the $N_{25}-H_{26}$ bond was allowed, and the angle formed by $C_{27}-N_{25}-H_{26}$ was unconstrained. This allowed for the guanidinium ion to hydrogen bond with the substrate throughout the reaction path. In acetic acid, the bond between $H_A$ and $O_{38}$ was unconstrained, and the plane defined by the two carboxylic oxygens and $C_{36}$ was allowed to rotate around the $C_{36}-C_{35}$ axis.

In mapping the energy surface for the reaction, a linear transit (LT) is defined between selected coordinates, the linear transit parameters, from an initial to a final value. At each transit point, the LT parameter is constrained, and the remaining coordinates are optimized, subject to the above-mentioned constraints. Thus, a LT calculation is a sequence of geometry optimizations along some selected reaction coordinate(s). Somewhat different constraints and different starting geometries were tested with similar results. Therefore, for succinctness in this paper, only calculations with the P−S distance as the reaction coordinate and the initial configuration specified by the values in Table 1 are presented. Note that these initial transit calculations are in the gas phase, but with critical protein residues providing a reasonable approximation to the environment. Of course, expanding the cluster would be better, but attempts at including the P-loop, for example, proved very expensive computationally.

**Combined Quantum-Continuum Electrostatics Calculations.** The self-consistent reaction field (SCRF) approach was used to model the effect of the charges and polarizability of all those parts of the protein not included in the quantum cluster. (Note that this SCRF approach is after the geometry optimization.) Li et al.[34] earlier presented the self-consistent reaction field (SCRF) procedure to include protein field contributions in electronic structure calculation. (We note a correction[35] to the earlier Li et al.[34] paper.) The present SCRF calculations were performed with the ADF (version 2000) code,[36] with these single point calculations following ADF (version 2.3)[26] linear transit calculations.

The SCRF procedure is briefly as follows. First, a gas-phase calculation is performed on the quantum cluster, and the atomic partial charges that best represent the molecular electrostatic potential are obtained, the so-called ESP charges. We followed the procedure followed by Li et al.[34] (See also ref 37.) The atomic radii used in the charge fitting calculations are 1.2, 1.4, 1.55, 1.7, 1.8, and 1.8 Å for H, O, N, C, S, and P atoms, respectively. Next, the Poisson equation is solved in a three-dielectric environment, with the cluster ($\epsilon = 1$) embedded in an electrostatic model representing the solvent ($\epsilon = 80$) and the rest of the protein ($\epsilon = 4$). The protein charges create what we term the protein field within the cluster,[34] and this is also obtained by solving the Poisson equation. The atomic radii for cluster atoms were as in the charge fitting procedure, and these radii are also nearly optimal in p$K_a$ calculations.[38] The protein partial charge distribution and atomic radii were based on the PARSE parameter set.[39] The continuum electrostatic calculations were performed using the MEAD[40,41] suite of programs. The Poisson equation was solved using the method of finite-differences on successively finer grids of size $91^3$, $91^3$, $111^3$ with linear spacings of 1.0, 0.5, 0.2 Å, respectively. The dielectric regions were delineated by their Connolly surfaces[42] using a probe radius of 1.4 Å.

The reaction field and protein field interact with the *true electron density*, and this effect is accounted for in the updated Hamiltonian. A new electron density distribution is computed on the basis of the updated Hamiltonian, new ESP charges and a new reaction field are computed, and the procedure is iterated to convergence. Typically, for the present system, the energies converge to within about 0.5 kcal/mol of final energies within three iterations. The final values reported here are converged to 0.1 kcal/mol which takes about six cycles. The free energy at the chosen transit point is then given by the sum of the gas-phase electronic energy and the free energy of interaction with the environment. The free energy at transit point $i$($W_i$) relative to a transit point chosen as the Michaelis complex or the ground state (see Results) is:

$$W_i = E_i + \Delta G_{env}(i) - E_{mc} - \Delta G_{env}(\mathrm{mc}) \qquad (1)$$

where mc denotes the Michaelis complex; $E_i$ is the (gas-phase) electronic energy; and $\Delta G_{env}(i) = {}^1/_2\int \rho_c \phi_{rxn} dV + \int \rho_c \phi_{prot} dV + E_{strain}$ is the free energy of interaction with the environment, where $\rho_c$ is the electronic charge density of the cluster, and $\phi_{rxn}$ and $\phi_{prot}$ are the reaction field and protein field, respectively. The integrals over $\rho_c$ are evaluated using the quadrature methods within ADF. $E_{strain}$ is the electronic distortion energy in the environment (see Appendix B for details).

In merging the quantum cluster back into the protein structure, the link hydrogens required special treatment (see, for example, ref 34). The link atoms $H_4$, $H_6$, $H_{39}$, and $H_{44}$ (Figure 1) were deleted in the charge fitting procedure. The atoms corresponding to these link hydrogens, Cys12-C, Cys12-N, Asp129-$C_\alpha$, and Ser19-$C_\alpha$, respectively, were restored in the protein. The link atom of the guanidinium group, $H_{26}$, bears a partial charge around +0.5 and was conserved as part of the QM region. Hence, the corresponding atom in the enzyme ($C_\delta$ of Arg 18), which has a partial charge of +0.35 according to the PARSE set, was removed from the protein. Prior to the self-consistent solvation calculations, the coordinates of the quantum cluster atoms were transformed back to the coordinates system of the protein using four stationary atoms (Cys12-$C_\alpha$, Cys12-$C_\beta$, Arg18-$N_\epsilon$, and Asp129-$C_\beta$) as reference. We also tested a slightly different approach whereby the

(33) Head, J. D.; Zerner, M. C. *Adv. Quantum Chem.* **1988**, *20*, 1.
(34) Li, J.; Nelson, M. R.; Peng, C. Y.; Bashford, D.; Noodleman, L. *J. Phys. Chem. A* **1998**, *102*, 6311.
(35) Liu, T.; Ullmann, M.; Noodleman, L. In the earlier work, a programming error led to the incorporation of the protein field after the completion of the self-consistent reaction field and protein field cycles. Thus, the magnitudes of the protein field and reaction field polarization term were substantially underestimated. However, this produces only modest changes in the calculated redox potentials.
(36) te Velde, G.; Bickelhaupt, F. M.; Baerends, E. J.; Guerra, C. F.; van Gisbergen, S. J. A.; Snijders, J. G.; Ziegler, T. *J. Comput. Chem.* **2001**, *22*, 931.
(37) Mouesca, J. M.; Chen, J. L.; Noodleman, L.; Bashford, D.; Case, D. A. *J. Am. Chem. Soc.* **1994**, *116*, 11898.
(38) Richardson, W. H.; Peng, C.; Bashford, D.; Noodleman, L.; Case, D. A. *Int. J. Quantum Chem.* **1997**, *61*, 207.
(39) Sitkoff, D.; Sharp, K.; Honig, B. *J. Phys. Chem.* **1994**, *98*, 1978.
(40) Bashford, D.; Gerwert, K. *J. Mol. Biol.* **1992**, *224*, 473.
(41) Bashford, D. In *Scientific Computing in Object-Oriented Parallel Environments*; Ishikawa, Y., Oldehoeft, R. R., Reynders, J. V. W., Eds.; Springer: Berlin, 1997; Vol. 1343 of *Lecture Notes in Computer Science*, pp 233−240.
(42) Connolly, M. *J. Appl. Crystallogr.* **1983**, *16*, 548.

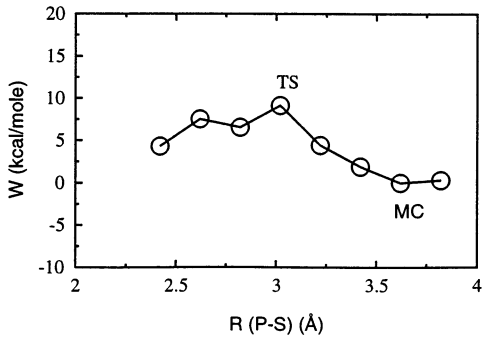


***Figure 2.*** Mechanism A energetics along the reaction coordinate. The transition state (TS) and Michaelis complex (MC) points are appropriately labeled. The forward direction of the reaction corresponds to the right-to-left direction along the plot.

link atoms are not deleted, but the corresponding protein atoms were. This, too, led to results similar to those reported here.

## 3. Results

Transition states in phosphoryl transfer reactions can occur along any position between the associative and dissociative extremes.[43] In the associative case, the bond to the attacking nucleophile is formed with no appreciable breakage of the bond to the leaving group, resulting in short bond lengths in the transition state, while at the dissociative extreme, the bond to the leaving group is broken with no appreciable bond formation to the incoming nucleophile, resulting in large bond lengths in the transition state. Between these extremes lies a concerted process, where bond breaking and bond formation go hand-in-hand.

**Mechanism A.** Figure 2 depicts the free energy change along the reaction coordinate, for a reaction path calculated assuming the protonation states of mechanism A. The computed barrier height is about 9.1 kcal/mol, whereas experimentally it is about 14 kcal/mol.[44] This agreement is reasonable considering that the experimental values for the energy profile were obtained using *p*-nitrophenyl phosphate as a substrate, rather than phenyl phosphate. On the basis of the free energy profile (Figure 2), we regard the second linear transit point as the Michaelis complex (the profile goes through a minimum at this point) and the fifth linear transit point as the transition state (the profile goes through a maximum at this point).

Figure 3 shows the progression of the P−$O_B$ bond cleavage along the reaction coordinate, the P−S distance. Starting from the initial reactant state in the lower right-hand corner, the reaction follows an almost linear path to the phosphoenzyme state in the upper left-hand corner. Thus, each incremental decrease of the P−S distance is accompanied by a nearly equal increase in the P−$O_B$ distance so that the S−$O_B$ distance remains nearly unchanged; in effect, a metaphosphate ($PO_3^-$) moves between the relatively stationary $O_B$ and S atoms.

Inspection of the bond lengths in the transition state (Figure 4) indicates a *dissociative* character: the forming- and breaking-bond lengths are large, and the transition state is loose. Notice also the proton transfer to the leaving group is nearly complete by the time the transition state is reached (lower panel in Figure 3 and Figure 4). Thus, our calculations predict that (a) the proton transfer is nearly complete in the transition state, and (b) a metaphosphate-like molecule is captured by the nucleophile *after* the proton transfer.

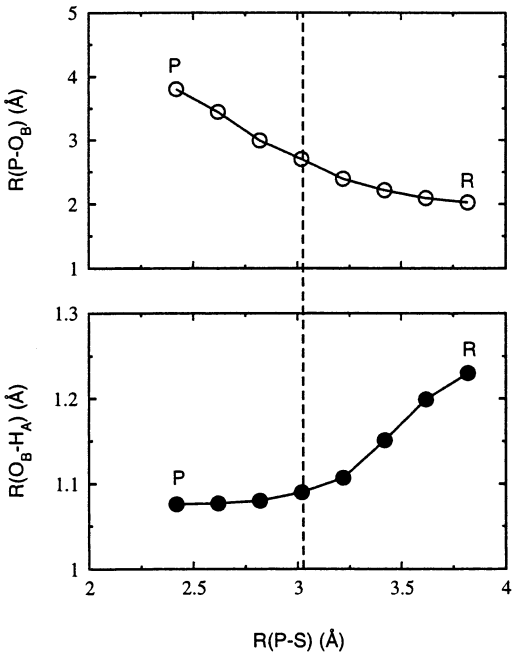


***Figure 3.*** Breaking of the substrate P−$O_B$ bond (top panel) and proton transfer to the leaving group as measured by R($O_B$−$H_A$) (bottom panel) along the reaction coordinate for mechanism A. The vertical dashed line marks the transition state. R and P refer to the reactant state and product state, respectively; thus the reaction proceeds from right to left across the plots.

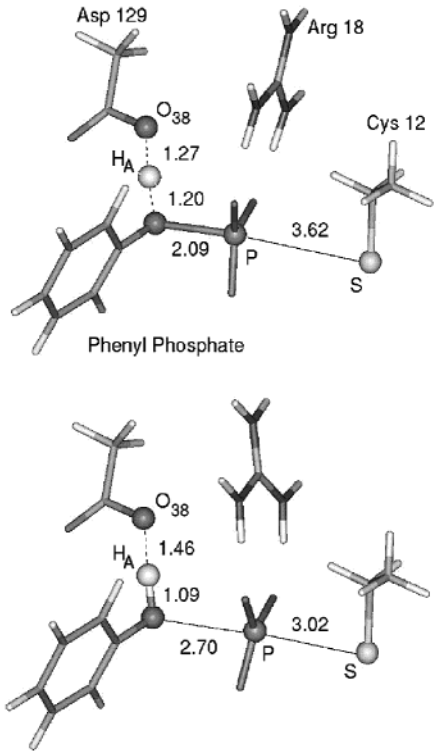


***Figure 4.*** Michaelis complex (top figure) and transition state (bottom figure) structures for mechanism A. For clarity, the Ser 19 residue has been deleted.

Figure 5 depicts the ESP charges on the relevant groups along the reaction coordinate. Comparing the gas-phase charges to

(43) Thatcher, G. R. J.; Kluger, R. *Adv. Phys. Org. Chem.* **1989**, *25*, 99.
(44) Zhang, Z. Y.; VanEtten, R. L. *J. Biol. Chem.* **1991**, *266*, 1516.

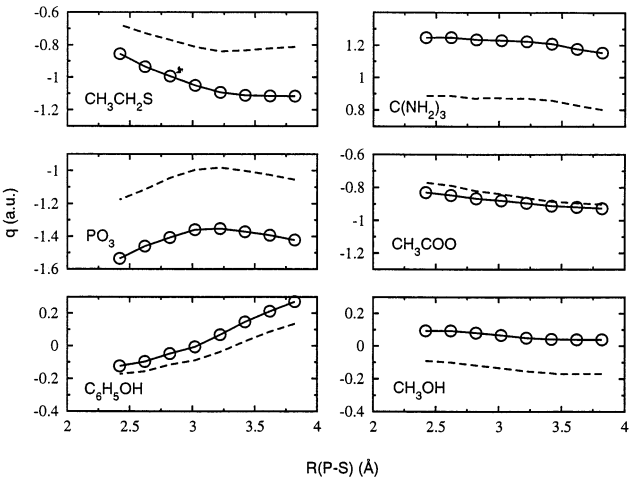


***Figure 5.*** ESP charge distribution on the relevant groups along the reaction coordinate for mechanism A. The dashed line is the ESP charge obtained in the gas-phase, that is, the initial cycle of the SCRF procedure. ○ denote the charges at the end of the SCRF procedure.

the charges at the final SCRF cycle, we can see that the SCRF procedure tends to concentrate negative charge on the metaphosphate and the ethanethiolate residues, with a loss of electron density for Arg 18 and Ser 19. Note that this is just the change between the initial cycle and final cycle of the SCRF procedure. Along the reaction coordinate, the change in charge on ethanethiolate between the Michaelis complex and the transition state is minimal (Figure 5). This suggests minimal interaction between the nucleophile and metaphosphate. This lack of nucleophilic interaction is consistent with a dissociative transition state (see, for example, ref 45). The charge on the metaphosphate is lower in the transition state than in the Michaelis complex, as would be the case for a dissociative transition state. The charge on the phenol leaving group changes to slight negative values past the transition state.

In considering atomic partial charges, it is imperative to emphasize that "charge" is not a direct quantum mechanical observable, and hence by necessity one has to use some *definition*. The ESP scheme used here is one such definition. Calculations using Mulliken charges (not shown) in the SCRF procedure lead to results qualitatively similar to those seen with the ESP model. However, the Mulliken charges are smaller in magnitude than the ESP charges.

**Mechanism B.** Figure 6 depicts the free energy change along the reaction coordinate. On the basis of the free energy profile, the third linear transit point is regarded as the Michaelis complex, and the seventh linear transit point is regarded as the transition state, respectively. The calculated barrier height of about 22 kcal/mol is 8 kcal/mol higher than the experimental estimate.[44]

For mechanism B, R(P−$O_B$) is nearly unchanged between the Michaelis complex and the transition state (Figure 7). In the transition state, the phosphorus is coordinated both with the thiolate and with the leaving group oxygen, apart from the nonbridge oxygens. The short bond lengths (Figure 8) and the presence of a pentacovalent phosphorane clearly suggest an associative transition state. Interestingly, the leaving group is *not* protonated in the transition state (Figure 8). Only when the

(45) Hengge, A. C. In *Comprehensive Biological Catalysis*; Sinnott, M., Ed.; Academic Press: New York, 1998; Vol. 1, pp 517−542.

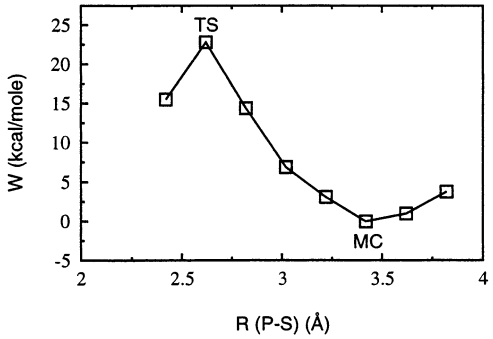


***Figure 6.*** Energetics along the reaction coordinate for mechanism B. The rest is as in Figure 2.

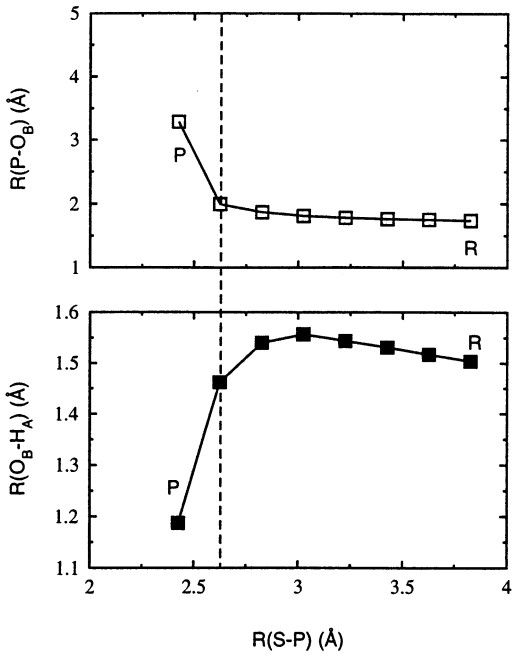


***Figure 7.*** Breaking of the substrate P−$O_B$ bond (top panel) and proton transfer to the leaving group as measured by R($O_B$−$H_A$) (bottom panel) along the reaction coordinate for mechanism B. The rest is as in Figure 3.

P−$O_B$ bond is cleaved is the proton transferred to the phenoxide anion (Figure 7).

The variation of charge on the thiolate between the Michaelis complex and the transition state (Figure 9) suggests a greater interaction between the thiolate and the substrate than in mechanism A, indicative of an associative transition state. The charge on the acid is minimally changed between the Michaelis complex and the transition state, again confirming the minimal change in interaction of the acid with the leaving group in the Michaelis complex and in the transition state. Note also that the charge on the phenol remains positive throughout, unlike the case for mechanism A where the charge changes to slight negative values after the transition state (Figure 5). We again note that calculations with Mulliken charges lead to similar trends along the reaction coordinate.

## 4. Discussion

Below, we discuss, in turn, our results for mechanisms A and B. Aspects of the calculation relating to the role of vibrational effects are collected together in Appendix A. Further, our methodology enables us to understand how the environment

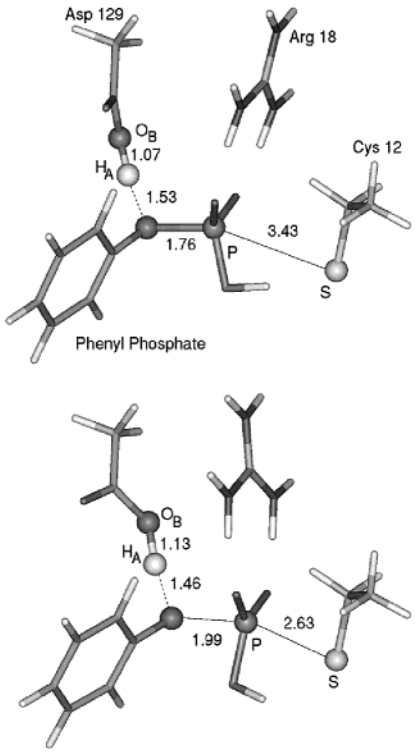


***Figure 8.*** Michaelis complex (top figure) and transition state (bottom figure) structures for mechanism B. The rest is as in Figure 4.

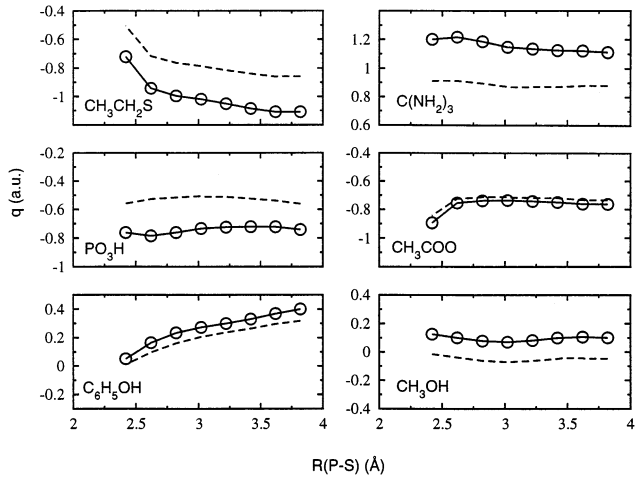


***Figure 9.*** ESP charge distribution on the relevant groups along the reaction coordinate for mechanism B. The rest is as in Figure 5.

impacts the computed barrier heights. This technical, albeit important, aspect of the present work is presented in Appendix B.

**Mechanism A.** The calculations predict an activation barrier of 9.1 kcal/mol (Figure 2), 5 kcal/mol less than the experimental estimate of 14 kcal/mol,[44] an encouraging level of agreement for calculations of such a complex system and the approximate treatment of the environment. Inclusion of vibrational effects, although desirable, is infeasible for systems as large as this one. Yet on the basis of studies of the dissociation of a model compound, methyl phosphate dianion, to methoxide plus metaphosphate anions, vibrational effects will likely lower the computed barrier height by another 1.5 kcal/mol (Appendix A). Another likely reason for the discrepancy is that the experimental values are based on a *p*-nitrophenyl phosphate substrate, whereas we used a phenyl phosphate substrate, which is more representative of a phosphorylated tyrosine than is *p*-nitrophenyl phosphate. The calculated reaction pathway is clearly dissociative (Figure 4). This dissociative transition state is predicted in the presence of Arg 18 (modeled as a guanidinium), which might have been expected to render the transition state more associative;[46] yet our calculations predict otherwise, in line with experimental studies showing that positive charge does not necessarily perturb the transition state structure.[47−49] Also noteworthy is the substantially advanced proton transfer to the leaving group in the transition state.

Kinetic isotope effect studies have been instrumental in understanding phosphoryl transfer mechanisms, both in bulk solution[50,51] and in proteins.[14,18,52−54] In phosphatases, these results have been interpreted to indicate, by comparison to their bulk solution counterparts, a dissociative transition state. In the transition state, the bond to the leaving group is largely broken with little bond formation to the nucleophile. Very advanced protonation of the leaving group (in the transition state) was also suggested by these results in the case of PTPases from Yersinia and rat PTP1[53] and the dual-specificity phosphatase VHR.[54] For the low molecular weight phosphatase, STP1, the isotope effects suggest a somewhat greater nucleophile−substrate interaction in the transition state, and the protonation of the leaving group is advanced, but not to the extent seen in other phosphatases.[52] Our structural results are in agreement with these experimental inferences and do show a well-advanced proton transfer to the leaving group. The slight negative charge on the leaving group also agrees with inferences based on isotope effects.[52]

Our structural predictions for mechanism A are in agreement with the predictions by Czyryca and Hengge[14] using semiempirical calculations. Our mechanism conflicts with structural results reported by Alhambra et al.[21] In their transition state for mechanism A, the P−S and P−O bond lengths are about equal and very short (∼2.3 Å). This is indicative of an associative transition state. We suspect the inadequate description of acid catalysis as the likely source of this discrepancy.

The role of acid catalysis deserves further exploration. As Hengge[45] notes, "general acid catalysis is another means to stabilize a phosphoryl transfer reaction, whether it occurs by an associative or dissociative transition state". Our calculations show that this acid catalysis partially neutralizes the −2 charge on the substrate to release a protonated leaving group and a −1 charged metaphosphate. This has two important consequences. First, the thiolate interacts with a −1 charged species, instead of a −2 charged species. Second, the protonation of the leaving group effectively precludes the back reaction, viz., the nucleophilic attack on the metaphosphate by phenol, a poor nucleo-

(46) Hassett, A.; Blattler, W.; Knowles, J. R. *Biochemistry* **1982**, *21*, 6335.
(47) Hoff, R. H.; Wu, L.; Zhou, B.; Zhang, Z. Y.; Hengge, A. C. *J. Am. Chem. Soc.* **1999**, *121*, 9514.
(48) O'Brien, P. J.; Herschlag, D. *J. Am. Chem. Soc.* **1999**, *121*, 11022.
(49) Herschlag, D.; Jencks, W. P. *J. Am. Chem. Soc.* **1987**, *109*, 4665.
(50) Cleland, W. W. *FASEB J.* **1990**, *4*, 2899.
(51) Hengge, A. C.; Edens, W. A.; Elsing, H. *J. Am. Chem. Soc.* **1994**, *116*, 5045.
(52) Hengge, A. C.; Zhao, Y.; Wu, L.; Zhang, Z. Y. *Biochemistry* **1997**, *36*, 7928.
(53) Hengge, A. C.; Sowa, G. A.; Wu, L.; Zhang, Z. Y. *Biochemistry* **1995**, *34*, 13982.
(54) Hengge, A. C.; Denu, J. M.; Dixon, J. E. *Biochemistry* **1996**, *35*, 7084.

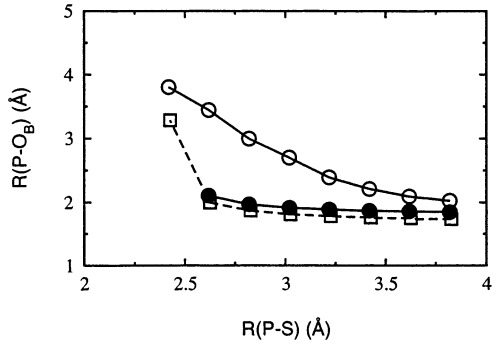


***Figure 10.*** Variation of R(P−$O_B$) along the reaction coordinate for mechanism A in the absence of acid catalysis. For comparison, the values for mechanisms A and B are also shown. ●, mechanism A without acid catalysis; ○, mechanism A; and □, mechanism B.

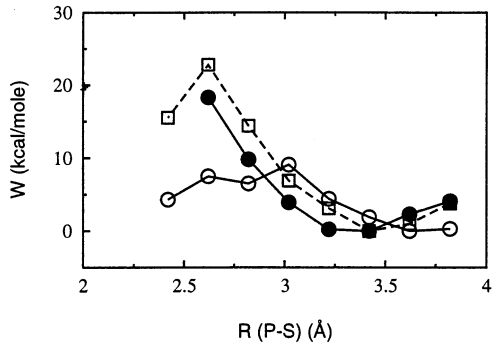


***Figure 11.*** Energetics along the reaction coordinate for mechanism A in the absence of acid catalysis. For comparison, the profiles for mechanisms A and B are also shown. ●, mechanism A without acid catalysis; ○, mechanism A; and □, mechanism B.

phile. A phenoxide anion, on the other hand, can effectively compete with the thiolate nucleophile.

The role of acid catalysis in stabilizing the dissociative transition state is also clearly illustrated by considering mechanism A in the absence of the acid. Figure 10 illustrates the progression of the P−$O_B$ bond cleavage along the reaction path in this case: *Absence of acid catalysis renders the transition state associative.* Beyond the last point shown in Figure 10 (left side, Figure 10), the leaving phenoxide anion is expelled and moves much farther away from the cluster, which would be precluded in the presence of a protein matrix. Around the last point, the bond breaking is quite abrupt, and we were unable to credibly calculate a transition state. Although the details of the path cannot be precisely modeled, the present calculations clearly show that in the absence of the acid, the transition state will have more associative character, a result that is consistent with experimental isotope effect data.[18]

From the calculated energetics for mechanism A in the absence of acid catalysis (Figure 11), it is clear that the loss of the acid results in a substantially greater activation barrier, comparable in magnitude to the trend observed for mechanism B, where acid catalysis occurs after the transition state. This trend is consistent with experimental trends that demonstrate the substantial decrease in substrate turnover by phosphatases upon mutation of the conserved acid (see, for example, refs 7, 9, 11). It is well-worth re-emphasizing the nature of the present "mutational" calculation: we take the initial configuration based on the presence of the acid and then remove the acid to generate a reaction pathway. This simplistic approach very likely misses the nuanced structural consequences of the Asp 129 mutation (in the real protein) which would impact the degree of associativeness observed in this study. Yet what does emerge from this study is the critical role played by the acid in promoting a rapid cleavage of the substrate leading to a dissociative pathway and the fact that absence of the acid will render the pathway somewhat associative, conclusions which are consistent with experimental isotope effects.[18]

**Mechanism B.** The results for mechanism B predict a barrier height of 22 kcal/mol. This is 13 kcal/mol higher than the mechanism A results and 8 kcal/mol higher than experimental estimates. As noted for mechanism A, heavy atom vibrational effects will tend to lower the barrier by about 1.5 kcal/mol. Aside from this, the transition state is clearly associative and involves a pentacovalent phosphorane. (As shown in Appendix A, vibrational effects along the proton-transfer pathway from the acid to the bridging oxygen will not change the nature of the transition state.) The modest degree of bond cleavage to the leaving group is similar to that expected in reactions of phosphate di- and triesters.[43] However, the experimentally observed isotope effects for the oxygen at the bridge position[14,52−54] are unlike those seen for phosphate di- and triester hydrolysis.[47,50] That is, isotope effects do not seem to suggest the presence of a phosphorane intermediate in phosphatases. Further, as noted in the Introduction, the pH-dependence of $k_{cat}/K_m$ suggests ionization states at variance with those used in mechanism B. On the basis of these considerations, we conclude that mechanism B (or B′) is unlikely.

## 5. Concluding Perspectives

The computed barrier heights, especially the much lower barrier height predicted for mechanism A *relative* to that for mechanism B, suggest that greater catalytic activity would result with a dianionic substrate than a monoanionic one, a preference in line with the experimental evidence reviewed in the Introduction. Further, the present calculations predict that in the enzyme−substrate complex examined here, the deprotonated substrate undergoes a dissociative mechanism, while the protonated substrate configuration examined here would react by an associative mechanism. For a more intuitive grasp of why this is so, we turn to some of the traditional classes of organic reaction mechanisms which have their analogues in phosphate chemistry.

We begin by constructing the obvious associative mechanism, Scheme 1, which is analogous to the $S_N2$ mechanism of carbon chemistry, but includes a proton transfer during the breakdown of the pentacovalent intermediate. Here, a nucleophilic attack forming a pentacovalent transition state is the initiating step. The question now is, how does the protonation state of the phosphate affect the nucleophilic attack? Protonating a nonbridging oxygen atom, as shown in this scheme, would make the phosphorus center more electrophilic than the deprotonated alternative, and thus more subject to nucleophilic attack. The expelled leaving group, the phenoxide anion, is only protonated by the general acid during the dissociation step. Scheme 1, in both its mechanistic steps and its most plausible substrate protonation, corresponds to our mechanism B in which a protonated substrate is assumed, and an associative, $S_N2$-like path results. This is inconsistent with experimental isotope effects[18] and is not the preferred mechanism predicted by the

***Scheme 1***

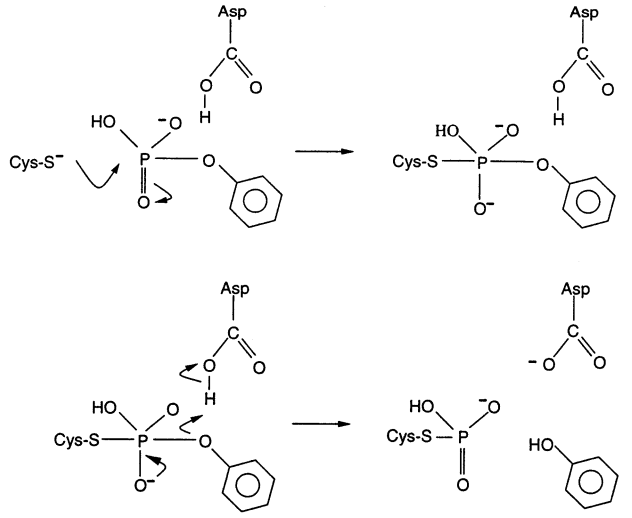


***Scheme 2***

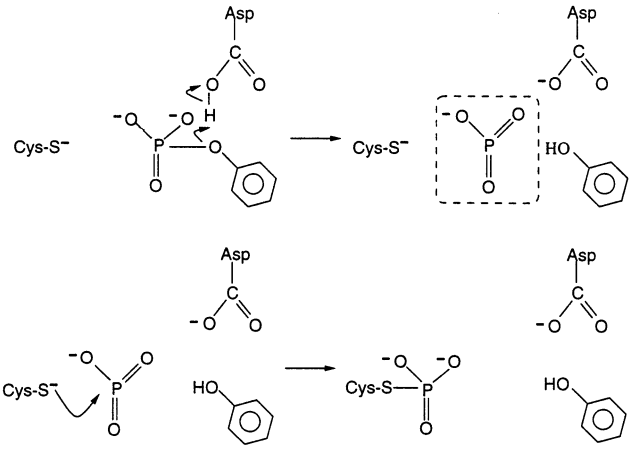


present calculations. It is worth emphasizing that in bulk solution the transition states for both the monoanion and the dianion hydrolysis are experimentally known to be dissociative, although it is somewhat more associative for the monoanion.[18] Yet enzymatic phosphoryl transfer reactions are nearly always dissociative and involve a dianionic substrate, which is consistent with the present calculation. Thus, the present calculations are not in conflict with experiments that emphasize the fact that the enzymes do not alter the dissociative nature of phosphoryl transfer reactions (see, for example, refs 47, 48).

We next construct a dissociative mechanism, Scheme 2, which has two steps: an acid-assisted elimination of a metaphosphate from the phenol (analogous to the EgA mechanism of carbon-center chemistry), followed by nucleophilic addition ($Ad_N$) of the metaphosphate to the thiolate. In this case, initiating the reaction with a deprotonated substrate, as shown in the scheme, is advantageous, as the proton transfer to a $-2$ charged species is more facile than that to a $-1$ charged species. Such a process would proceed via a dissociative transition state. This scheme corresponds to our mechanism A, in which a deprotonated substrate is assumed, early proton transfer to the leaving group occurs, and a dissociative transition state results. Note also that the nucleophilic attack is by a $-1$ charged thiolate nucleophile on a $-1$ charged metaphosphate. Hence, in terms of electrostatic repulsion between the interacting species, it is no worse than that expected for Scheme 1. Thus, the present calculations strongly support the conclusion that the energetically favorable mechanistic pathway involves reaction of the bound dianion of substrate and that the mechanism is highly dissociative.

**Acknowledgment.** D.A. thanks Christin Thomas (Purdue University) for helpful discussions on the protonation state of the substrate. D.A. and D.B. gratefully acknowledge funding from the NIH (grant # GM-45607), R.L.V.E. gratefully acknowledges funding from NIH DHHS (grant # GM-27003), and L.N. gratefully acknowledges funding from NIH grants GM43278 and GM39914.

## Appendix A

In the Discussion, we briefly alluded to vibrational effects and their impact on calculated barrier heights. In principle, inclusion of such effects could impact the evolution of the reaction, but, as we show below, this is unlikely for the present system. To estimate the vibrational contributions, we consider a model system involving the reaction of methyl phosphate dianion:

$$CH_3OPO_3^{2-} \rightarrow CH_3O^- + PO_3^-$$

This is taken as a prototype for the reaction involving the dianionic substrate considered in the main text for the purpose of estimating upper bounds on vibrational effects. We identified the transition state for this reaction using the synchronous transit-guided quasi-Newton method as implemented in the QST3 procedure within the Gaussian package.[31] The calculations were at the B3LYP/6-31+G(d,p) level of theory. Once the transition state was identified and confirmed by a frequency analysis, we find that zero-point effects contribute only about 1.5 kcal/mol toward lowering the barrier height. Thus, for this dissociative process, the one for which vibrational effects are likely to be most severe, the contribution toward barrier lowering is quite modest.

Yet there remains the question of vibrational effects along the proton-transfer pathway from the acid to the bridging oxygen. Clearly, in mechanism A, where we already predict an advanced proton transfer to the bridging oxygen in the Michaelis complex, inclusion of proton vibration will only hasten this process. Thus, in this instance, the mechanistic conclusions will not be altered.

For mechanism B (see Scheme 1), we calculated proton-transfer energetics for transferring the proton from the base to the bridging oxygen. These calculations are similar to our cluster calculations, having the same active-site model, but the transit parameter is now a measure of the proton-transfer step: the acid hydrogen to bridging oxygen ($O_B-H_A$) distance. The linear transits were performed for the cluster configurations corresponding to the Michaelis complex and the transition state. The constraints on the cluster were as before (Methods section), but the P−S bond distance is kept constrained to the respective values shown in Figure 8 for the Michaelis complex and the transition state. This ensured that (a) two slices through a realistic two-dimensional free energy surface are being explored, with $R(O_B-H_A)$ and the already considered (main text) R(P−S) as the two axes, and (b) the breaking bond $P-O_B$ is free to evolve under the influence of the transferring proton.

The energetics are illustrated in Figure 12. In the MC, bond cleavage, as measured by $R(P-O_B)$, is negligibly altered by

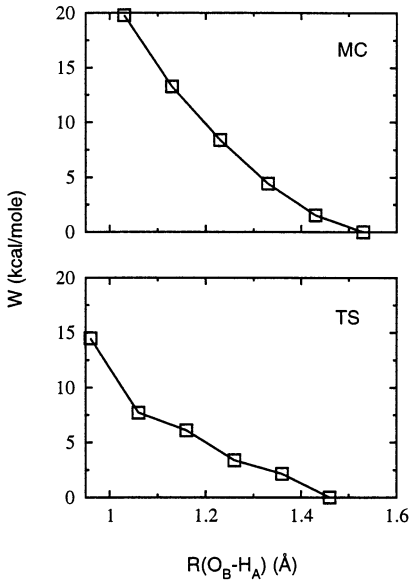


***Figure 12.*** Energetics along the reaction coordinate defined by R($O_B$−$H_A$) (Figure 1). In the graphs above, the reaction progresses from right to left.

***Table 3.*** Components of the Free Energy of Interaction with the Environment (Eq 2) and the Gas-Phase Electronic Energies for Mechanisms A and B (in kcal/mol)[a]

| state | $E_{gas}$ | $E^{i}_{prot}$ | $E^{pol}_{prot}$ | $E^{i}_{rxn}$ | $E^{pol}_{rxn}$ | $E_{strain}$ | total |
|---|---|---|---|---|---|---|---|
| | | | Mechanism A | | | | |
| MC | −6408.0 | −72.0 | −105.9 | −174.8 | −68.5 | 90.2 | |
| TS | −6408.7 | −69.6 | −103.8 | −172.9 | −62.1 | 87.1 | |
| Δ | −0.7 | 2.4 | 2.1 | 1.9 | 6.4 | −3.1 | 9.0 |
| | | | Mechanism B | | | | |
| MC | −6550.6 | −41.7 | −98.7 | −76.5 | −37.5 | 70.9 | |
| TS | −6536.2 | −34.4 | −99.3 | −75.6 | −37.3 | 71.4 | |
| Δ | 13.8 | 7.3 | −0.5 | 0.9 | 0.2 | 0.5 | 22.0 |

[a] Δ gives the difference between the Michaelis complex (MC) and the transition state (TS). See Methods for a definition of various terms.

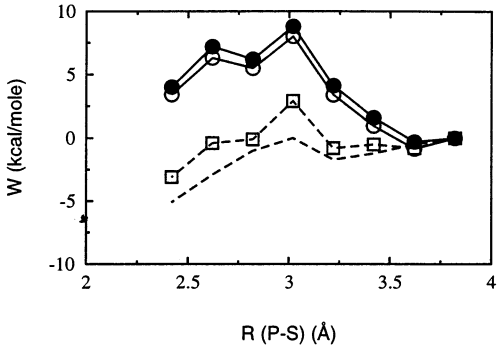


***Figure 13.*** Comparison of different models for environment effects in mechanism A. ●, full-SCRF; ○, SCRF scheme terminated after one cycle; □, electron density as in the gas phase (initial cycle); bare dashed line, initial cycle with interaction calculated with point charges rather than quadrature over density.

the proton transfer (not shown). In the TS, R(P−$O_B$) marginally increases from about 2 Å (Figure 8) to about 2.3 Å (not shown).

Clearly, the barrier to transferring the proton is substantial. Note that, as before, these cluster calculations, including environmental effects, do not include vibrational effects. Yet even estimating as an upper bound a 5 kcal/mol barrier-lowering effect due to proton vibrations, we observe a substantial barrier. This suggests that inclusion of vibrational effects along the proton-transfer pathway from acid to bridging oxygen will not change the finding that in mechanism B, proton transfer occurs well after the transition state.

## Appendix B

To illustrate the role of polarization effects, the free energy of interaction with the environment, $\Delta G_{env}$, can be decomposed as (see also Li et al.[34]):

$$\Delta G_{env} = (E^{f}_{elec} - E^{i}_{elec}) + E^{i}_{prot} + (E^{f}_{prot} - E^{i}_{prot}) + \Delta G^{i}_{rxn} + (\Delta G^{f}_{rxn} - \Delta G^{i}_{rxn})$$

$$= E_{strain} + E^{i}_{prot} + E^{pol}_{prot} + E^{i}_{rxn} + E^{pol}_{rxn} \quad (2)$$

The superscripts "f" and "i" refer to the final and initial steps, respectively, of the self-consistent reaction field cycle, and thus "i" corresponds to the cycle in the gas phase. $E^{j}_{prot}$ and $\Delta G^{j}_{rxn}$ are, respectively, the interaction energy of the protein with the cluster and the reaction field contribution to $\Delta G_{env}$with charges obtained at the *j*th self-consistent cycle. $E_{strain} = E^{f}_{elec} - E^{i}_{elec}$ is the change in electronic energy and is a measure of the energy associated with the deformation of the electron density from its gas-phase distribution to that in the protein. Let the difference between the self-consistent densities in the protein−solvent environment and the gas-phase environment be defined as the "polarization density". This polarization density is generated by the sum of the reaction field and protein field potentials. Then $E^{pol}_{prot} = E^{f}_{prot} - E^{i}_{prot}$ and $E^{pol}_{rxn} = \Delta G^{f}_{rxn} - \Delta G^{i}_{rxn}$ are then, respectively, the energy associated with the polarization density interacting with the protein field and the difference in reaction field energy between the final and initial electron densities.

Table 3 gives the components of the free energy of interaction of the cluster with the environment according to eq 2. $E^{i}_{prot}$, the interaction energy of the cluster with the protein, is more stabilizing for mechanism A than for mechanism B, a consequence of the greater overall negative charge in mechanism A. The change (Δ) in $E^{i}_{prot}$ between the Michaelis complex and the transition state is more positive for mechanism B, indicating that the protein does not adequately stabilize the monoanionic substrate in the transition state. This is the second largest contribution to the barrier height for mechanism B, the first being the change in the gas-phase energy itself. For mechanism A, the largest contribution to the barrier height comes from the change in $E^{rxn}_{pol}$, the polarization energy of the altered electron density interacting with the reaction field. This effect is attributable to the fact that in the Michaelis complex, formally a −2 charge is concentrated on the substrate, whereas in the transition state, this charge is distributed on the metaphosphate and on the conjugate base of Asp 129. However, the same effect also leads to a favorable change in $E_{strain}$. For the associative mechanism B, $E_{strain}$ hardly changes, as there are no bond-breaking events between the Michaelis complex and the transition state.

In the SCRF procedure, the true electron density interacts with the protein field and also with the reaction field generated by the atom-centered charges on the quantum cluster. The importance of this can be seen by considering the interaction of the protein field and the reaction field with the atom-centered point charges themselves, with no self-consistent relaxation of electron density carried out. (This is the so-called rigid charge

model.[55]) This rigid charge model leads to severe underestimation of the barrier height (Figure 13, bare dashed line). Performing the quadratures − recall that $\Delta G_{env}(i) = {}^1/_2\int \rho_c \phi_{rxn}\, dV + \int \rho_c \phi_{prot}\, dV$ (here $E_{strain}$ is zero) − with the gas-phase electron density alone somewhat improves the computed barrier height (giving 3.7 kcal/mol, see □ plot in Figure 13). However, performing just one full cycle of the SCRF (○) recovers a substantial portion of the fully converged SCRF profile (●), illustrating the importance of the relaxation of the electron density from the gas-phase value and the proper accounting of its interaction with the macroscopic fields.

(55) Tomasi, J.; Persico, M. *Chem. Rev.* **1994**, *94*, 2027.

JA020046N